Journal of Glaciology, Vol. 22, No. 86, 1979

GRAIN COARSENING OF WATER-SATURATED SNOW

By CHARLES F. RAYMOND

(Geophysics Program, University of Washington, Seattle, Washington 98195, U.S.A.)

and KATSUTOSI TUSIMA

(Institute of Low Temperature Science, Hokkaido University, Sapporo, Japan 060)

ABSTRACT. Experimental measurements were made of changes in grain-size distribution with time in snow saturated with solutions of various impurity contents. Qualitatively, the changes in grain-size distribution occur by shrinkage and eventual disappearance of the relatively small particles and growth of the relatively large particles by a solid mass-exchange process which conserves the total solid mass. The distribution of relative grain size is found to be essentially time independent except for transient effects lasting only several to several tens of hours after the time of initial saturation. Mean grain volume increases at a constant rate, which for solutions of impurity concentration less than about 0.01 mol l^{-1} is $(5 \text{ to } 6) \times 10^{-3}$ $mm^3\ h^{-1}$. In pure solutions the smallest particles shrink at a characteristic rate of about 1×10^{-2} $mm^3\ h^{-1}$. Once the steady relative-size distribution is established, the rate of volume change of typical grains varies linearly with grain volume from the characteristic negative rate for the smallest particles through zero for particles of mean volume to positive values for particles of larger volume. The basic features of the changes that take place are explained in terms of heat-flow controlled melting and freezing determined by temperature differences associated with the effect of particle surface curvature on melting temperature. The constant rate of increase of mean grain volume is a consequence of conservation of total ice volume. The expectation that particles of intermediate size would be neither shrinking or growing leads to the conclusion that the actual rate of increase in mean grain volume is about one-half the characteristic melting rate of the smallest particles, which fits the observations. The process of grain growth is slowed by impurities in a way which can be predicted from the melting-temperature depression caused by the impurity and its diffusion coefficient. The transport of heat between grain surfaces is largely through the liquid-filled gaps between them, but about 19% is conducted through the solid.

RÉSUMÉ. *Le grossissement des grains de la neige saturée en eau.* On a mesuré expérimentalement la variation avec le temps de la répartition des dimensions des grains dans la neige saturée avec des solutions de différentes teneurs en impuretés. Qualitativement les changements dans la répartition des dimensions des grains se produisent par réduction et éventuellement par disparition des particules relativement petites et grossissement des particules relativement grandes au cours d'un processus d'échange de matière qui conserve la masse totale. La distribution de la dimension relative des grains apparaît comme essentiellement indépendante du temps à l'exception des effets transitoires qui retardent de seulement quelques dizaines d'heures le moment de l'équilibre après le moment de la saturation initiale. Le volume moyen du grain augmente à un rythme constant qui, pour des solutions de concentration en impuretés inférieures à environ 0,01 mol l^{-1}, est de 5 à 6×10^{-3} $mm^3\ h^{-1}$. Dans des solutions pures, les plus petites particules décroissent à une vitesse caractéristique d'environ 1×10^{-2} $mm^3\ h^{-1}$. Une fois qu'un état relatif de stabilité de la distribution a été atteint, la vitesse de changement de volume des grains moyens varie linéairement avec le volume du grain depuis la décroissance caractéristique des plus petits grains, en s'annulant pour les particules de taille moyenne jusqu'à la croissance pour les particules de plus gros volume. Le comportement de base des changements constatés s'explique par un mécanisme de gel et dégel contrôlé par le flux thermique à partir des différences de températures et avec l'effet de la courbure superficielle des grains sur la température de fusion. La vitesse constante d'accroissement du grain moyen est une conséquence de la conservation du volume total de glace. Le fait que l'on s'attende à ce que les particules de taille intermédiaire ne doivent ni décroître ni croître conduit à la conclusion que la vitesse réelle de croissance de la taille du grain moyen est environ la moitié de la vitesse caractéristique de fusion des plus petits grains, ce qui corrobore les observations. Le processus de croissance des grains est ralenti par les impuretés d'une manière qui peut être prévue à partir de la diminution de la température de fusion entraînée par la présence des impuretés et leur coefficient de diffusion. Le transport de chaleur entre les surfaces des grains se fait en grande partie par le liquide qui remplit les vides entre eux, mais environ 19% de cette chaleur transite à travers le solide.

ZUSAMMENFASSUNG. *Kornvergröberung in wassergesättigtem Schnee.* Die zeitliche Änderung der Korngrössenvertailung in Schnee, der mit Lösungen verschiedenen Verunreinigungsgrades gesättigt war, wurde experimentell gemessen. Qualitativ erfolgen diese Änderungen durch Schrumpfen und eventuelles Verschwinden der relativ kleinen Partikel und Anwachsen der relativ grossen auf dem Wege eines Austauschprozesses fester Massen, bei dem die Gesamtheit der festen Masse erhalten bleibt. Die Verteilung der relativen Korngrösse ergibt sich im wesentlichen als zeitunabhängig, mit Ausnahme von Übergangserscheinungen, die nur einige oder einige 10 Stunden nach dem Zeitpunkt der anfänglichen Sättigung andauern. Das mittlere Kornvolumen wächst mit konstanter Geschwindigkeit, die für Lösungen mit einer Verunreinigungskonzentration von weniger als etwa 0,01 mol l^{-1} $(5 \text{ bis } 6) \times 10^{-3}$ $mm^3\ h^{-1}$ beträgt. In reinen Lösungen schrumpfen die kleinsten Partikel mit einer charakteristischen Geschwindigkeit von etwa 1×10^{-2} $mm^3\ h^{-1}$. Ist einmal die stationäre relative Grössenverteilung erreicht, so pendelt die Geschwindigkeit der Volumenänderung typischen Körner linear mit dem Kornvolumen zwischen der charakteristischen negativen Geschwindigkeit für die kleinsten Partikel über Null für Partikel mittleren Volumens zu positiven Werten für Partikel grossen

Volumens. Die grundlegenden Erscheinungen der auftretenden Veränderungen lassen sich durch Schmelz- und Gefriervorgänge unter Wärmefluss erklären, die durch Temperaturdifferenzen, verbunden mit der Wirkung der Oberflächenkrümmung der Partikel auf die Schmelztemperatur, bestimmt werden. Die konstante Geschwindigkeit der Zunahme des mittleren Kornvolumens ist eine Folge der Erhaltung des Gesamtvolumens des Eises. Die Erwartung, dass Partikel mittlerer Grösse weder schrumpfen noch wachsen würden, führt zu dem Schluss, dass die tatsächliche Geschwindigkeit der Zunahme des mittleren Kornvolumens ungefähr halb so gross ist wie die charakteristische Schmelzgeschwindigkeit der kleinsten Partikel, was mit den Beobachtungen übereinstimmt. Der Vorgang des Kornwachstums wird durch Verunreinigungen verlangsamt, und zwar auf eine Weise, die aus der Senkung der Schmelztemperatur infolge der Verunreinigung und ihrem Diffusionskoeffizienten vorausberechnet werden kann. Der Wärmetransport zwischen den Kornoberflächen erfolgt grösstenteils über die flüssigkeitserfüllten Lücken zwischen ihnen, doch werden etwa 19% der Wärme durch die feste Phase geleitet.

1. Introduction

Dry deposited snow experiences gradual changes in texture as a result of metamorphic processes controlled largely by diffusion of water vapor in the void spaces (Hobbs, 1968). When liquid phase is introduced into snow, the rate of metamorphism is greatly accelerated in comparison to dry conditions (Wakahama, 1965, 1968, [1975]). The rapid changes caused by wetting can be of major importance in the initiation of avalanches (Mellor, 1968), over-snow transport of men or vehicles, alteration of stratigraphy in an isothermal snow-pack and the pattern of water percolation (Colbeck, 1972), and the densification of snow or firn into ice (Anderson and Benson, 1963). One important textural change is a rapid increase in mean grain size. This paper gives quantitative experimental data on the rate of grain-size change in dry deposited snow which is suddenly saturated with water solutions of various impurity contents and explains these results in terms of a local melting and freezing process controlled by heat exchange between particles such that small ones melt and large ones freeze. At an advanced stage of growth only a small percentage of the original snow particles remain and the major portion of their volume has been slowly frozen from the liquid phase. Because of the preferential partitioning of impurities to the liquid phase and possible isotope fractionation on freezing, the process can have major consequences for the chemistry of the snow.

The heat-diffusion controlled process of grain growth in water-saturated snow is somewhat analogous to changes in precipitate particles in fluid or solid solutions caused by mass diffusion between the particles, a process sometimes referred to as Ostwald ripening. This kind of process has been examined theoretically for the case when the particles are dispersed and exchange mass only indirectly by interaction with the solution (Greenwood, 1956; Lifshits and Slyozov, 1961) and has various applications, examples of which are the growth of dispersed water droplets in the atmosphere, second phase particles in metals, and crystals in hydrothermal or high-temperature metamorphism of some rocks (Chai, 1973). Of possible glaciological importance is the behavior of possible solid inclusions of slightly soluble impurities expected in cold polar ice below eutectic temperatures (Paren and Walker, 1971). The experimental results and analysis for grain growth in water-saturated snow in which ice particles are in direct contact with neighboring ones can provide a model for extending these theories to conditions of closely packed particles as exist in dry or wet snow or gravity settled crystal cumulates in solutions or magmas.

2. Experimental results

The results of two types of experiments are summarized in this section. The first part describes the changes in grain-size distribution in a bulk snow sample saturated with water. Additional details about these experiments are to be published in a further paper by K. Tusima. The second part describes direct observation of the rate of volume change of individual ice particles in various environments simulating types of conditions which exist in bulk snow. Some of these results are from new experiments and some are from measurements made on already existing time-lapse movies of wet-snow metamorphism (Wakahama, [1975]).

2.1. *Water-saturated bulk snow*

Experimental method

A sample was prepared by saturating about 400 g of dry, natural, new snow with about 500 ml distilled, de-ionized water or prepared solution of known concentration of a specific solute (NaCl, glucose, HCl, or dextran). Before mixing the snow and fluid solution, they were both brought to within 1 deg of 0°C. Properties of samples used in the experiments are listed in Table I.

TABLE I. SUMMARY OF EXPERIMENTS

No.	*Impurity concentration* mol/kg H_2O	*Sampling times* hours after saturation	*Environment*
Distilled water			
1	<0.002	1, 2, 5, 10, 20, 30, 40, 50, 70, 80, 100, 130, 170	0°C chamber
2	<0.002	1, 2, 5, 10, 20, 30, 50, 70, 100, 130, 150	0°C chamber
3	<0.002	1, 2, 5, 10, 20, 40, 60, 80, 110	0°C chamber
4†	<0.002	1, 2, 5, 10, 30, 50, 60, 80, 100	0°C chamber
5†	<0.002	1, 2, 5, 10, 20, 30, 50, 70, 100, 130, 150	0°C chamber
NaCl solution			
6	1.7×10^{-4}	1, 2, 5, 10, 20, 30, 40, 50, 70, 80, 100, 130, 170	0°C chamber
7	1.7×10^{-3}	1, 2, 5, 10, 20, 30, 40, 50, 70, 80, 100, 130, 170	0°C chamber
8	0.017	1, 2, 5, 10, 20, 30, 40, 50, 70, 80, 100, 130, 170	0°C chamber
9	0.017	1, 2, 5, 10, 20, 30, 50, 70, 150	0°C chamber
10	0.1	0.5, 1, 2, 5, 10, 20, 30, 50, 58, 70, 80, 100	Dewar flask
11*	0.17	1, 2, 5, 10, 20, 30, 40, 50, 70, 80, 100, 130, 170	0°C chamber
12	1.0	0.08, 1, 5, 20, 31.5, 53.75, 101	Dewar flask
Glucose solution			
13	0.01	1, 2, 5, 10, 20, 40, 60, 80, 110, 170	0°C chamber
14	0.01	5, 10, 25, 35, 50, 60, 76, 100, 150, 180, 201, 348	0°C chamber
15	0.1	1, 5, 10, 20, 40, 60, 80	0°C chamber
16	0.1	5, 10, 25, 35, 50, 60, 76, 100, 150, 180, 201	0°C chamber
17	0.1	1, 5, 10, 20, 32, 50, 70.5, 80, 100, 120, 200, 408, 552	Dewar flask
18*	0.5	1, 2, 5, 10, 20, 40, 60, 80, 110	0°C chamber
19	0.94	15.13, 30, 80, 110, 131, 195, 252, 276, 298	Dewar flask
20	2.0	1, 5, 10, 20, 32, 50, 70.5, 80, 100, 120, 300	Dewar flask
HCl solution			
21*	0.34	1, 5, 10, 20, 32, 50, 70.5, 80, 100	0°C chamber
22*	0.67	0.5, 1, 2, 5, 10, 20, 30, 50, 58, 70, 80, 100, 120	0°C chamber
Dextran solution			
23	*c.* 7×10^{-4}	0.5, 1, 2, 5, 10, 20, 30, 50, 58, 70, 80, 100, 120, 150	0°C chamber

* Noticeable loss of ice mass during experiment.
† Forced water circulation through sample.

The samples were aged in two different types of controlled environment designed to minimize heat exchange with the surroundings. Samples made with distilled water or solution of concentration less than 0.7 mol kg^{-1} were prepared in 1 l acrylic containers with sealable lids and were kept in a 0°C chamber surrounded by several layers of coarse crushed ice soaked with distilled water and insulation. Samples with solution concentration larger than 0.7 mol kg^{-1} were placed in Dewar flasks of volume 3.6 l with lids. In either case, the apparatus was in a cold room with temperature controlled close to 0°C.

The net mass change of samples made with distilled water was examined by placing a control sample in a special container in the same 0°C chamber. The control sample mass was about 500 g of ice. The container had an O-ring sealed lid with a capillary tube of 2 mm inner diameter extending above it. Any change in total volume of the control ice sample

https://doi.org/10.3189/S0022143000014076 Published online by Cambridge University Press

could be sensed by changes in water level in the capillary tube. The fractional change in total ice volume was found to be less than 2×10^{-4} h^{-1} or about 0.04 over the typical 200 h span of the experiments. Therefore, the ice mass of samples prepared with distilled water remained nearly constant.

The ice mass loss of samples prepared with soluble impurities was not directly tested. It is likely that there was some net loss by melting for those experiments carried out in the 0°C chamber, because of depression of the sample temperature by impurities. However, no noticeable mass loss was observed except in the case of experiment numbers 28, 27, 17, and 5 listed in Table I. Samples in Dewar flasks probably suffered insignificant net ice mass loss. In the cases when heat did flow to the sample, it is likely that melting occurred only on the surface of the sample without significant alteration of the course of texture change in the interior of the sample.

The size distribution of a sample was examined at the times given in Table I by scooping from it a small subsample of about 0.5 g total ice weight. This subsample was then immediately disaggregated, spread out, and photographed using a microscope and 35 mm camera set up to give a magnification of about 5× on the camera focal plane. To measure the size distribution of subsamples, the 35 mm film images were printed at enlarged scale to give a total magnification usually of about 20×. The mean diameter of each particle image was measured using a Leitz KG-2 size analyzer. The size analyzer counts the number of images in diameter intervals with equally spaced boundaries 0.55 mm apart, which corresponds to a spacing of 0.028 mm at the typical real scale. The number of particles in each 0.028 mm size interval constitute the basic data of the experiment.

Description of sample evolution

Figure 1 shows the appearance of parts of disaggregated subsamples taken at various times in experiment 1 (Table I). Within several tens of minutes the initially irregular particles of new snow are subspherical. After desegregation these are either isolated or bonded together in small groups by unbroken necks at contacts between particles. The morphology of the particles and their appearance under crossed polaroids shows that they are single crystals. The mean size of the particles increases progressively with time, which is usually described as grain coarsening. The same qualitative behavior exists for all of the experiments performed.

The mean volume $\bar{v}$ of particles in the sample can be expressed as

$$\bar{v} = \frac{V}{N}, \tag{1}$$

where V is the total ice volume of the sample and N is the total number of particles. In these experiments V is essentially constant, and differentiation of Equation (1) gives

$$\frac{\mathrm{d}\bar{v}}{\mathrm{d}t} = -\bar{v}\,\frac{1}{N}\,\frac{\mathrm{d}N}{\mathrm{d}t}. \tag{2}$$

The increase of mean size occurs by reduction of N, so that the constant ice volume is partitioned between fewer particles. The only process causing changes in N is shrinkage of particles to zero volume, which is described in Section 2.2. The definition of particles and the way of counting them eliminates combination of two or more particles as a process for reduction of N. Time-lapse photography of the process made previously (Wakahama, [1975]) demonstrates this clearly, and also shows no evidence for splitting of particles or nucleation of new particles, which in any case would not be expected on physical grounds. The particles change their size continuously and at any time the large ones are getting larger and the small ones smaller.

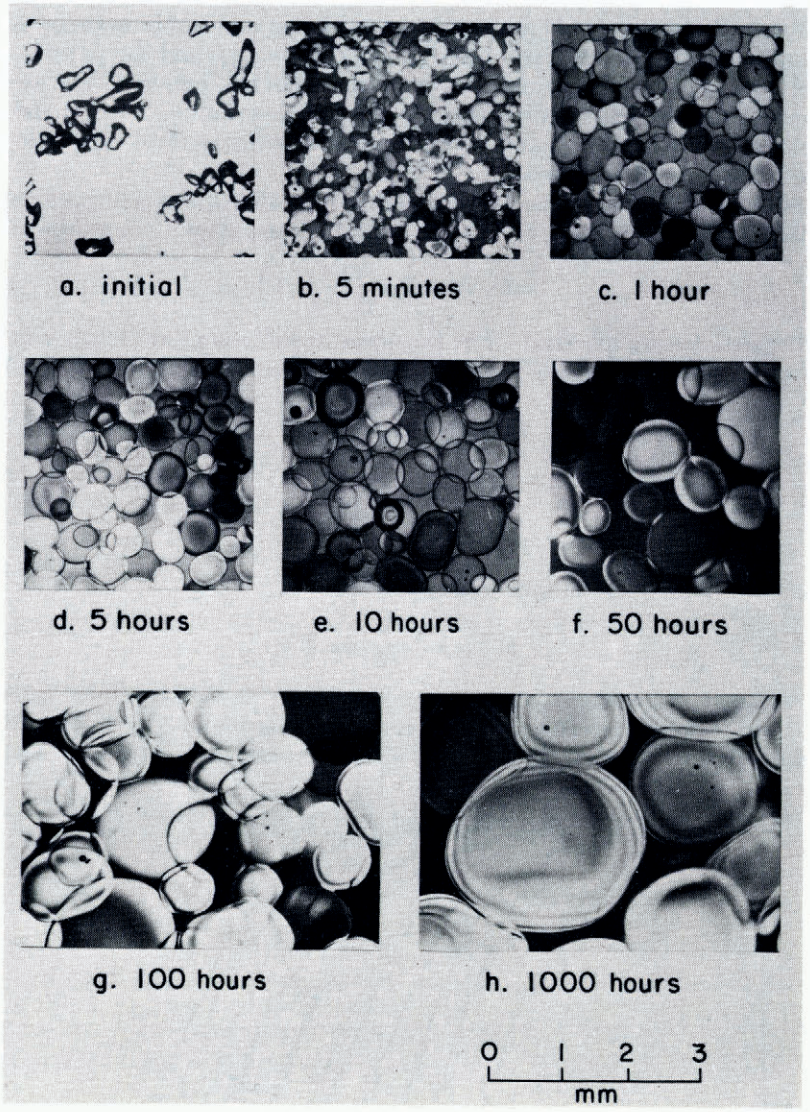

Fig. 1. Photomicrographs of snow particles at various times after saturation with distilled water. Experiment 1.

Properties of size distributions

The size distribution of particles in a subsample may be described by the cumulative distribution Ψ, which is the fractional number of particles with size greater than or equal to a specific size. These cumulative distributions decrease monotonically from a value of 1 at zero size to a value of 0 for sizes larger than the biggest particle. Although it is more conventional to define cumulative size distributions in terms of the fractional number strictly smaller than a specific size, the above definition is more convenient for analysis of these experiments.

Strictly speaking Ψ is a step function with discontinuity at the size of each particle. Because of the measurement method of counting particles in discrete size intervals described above, our actual knowledge of the distribution has discontinuities at the interval boundaries.

https://doi.org/10.3189/S0022143000014076 Published online by Cambridge University Press

However, we shall assume that Ψ is continuous, which is reasonable because the number of particles in each subsample was fairly large (usually about 500) and the particle sizes within a size interval were probably fairly uniformly spread within the interval. Also we shall assume that the subsample distribution describes the sample distribution, so that the sequence of subsamples collected at various times during a single experiment shows the change of the size distribution of the sample with time.

We shall use particle diameter d and volume v as alternative size parameters and the corresponding distributions $\Psi_d(d, t)$ and $\Psi_v(v, t)$ which are simply related by

$$\Psi_v(v, t) = \Psi_d\left(\left(\frac{6v}{\pi}\right)^{\frac{1}{3}}, t\right), \tag{3}$$

assuming the particles are spherical. The fractional number of particles per unit size interval is given by the negative slope of Ψ, so frequency distributions ϕ may be defined as

$$\phi_d(d, t) = -\frac{\partial \Psi_d(d, t)}{\partial d}, \tag{4a}$$

and

$$\phi_v(v, t) = -\frac{\partial \Psi_v(v, t)}{\partial v}. \tag{4b}$$

From Equation (3) these are simply related by

$$\phi_v(v, t) = \frac{2}{\pi d^2}\phi_d(d, t). \tag{5}$$

Figure 2 shows Ψ_d measured for subsamples taken at various times in experiment 1 (Table I). On a logarithmic scale of diameter, the size distributions at different times all have about the same shape. After the first 10 h the differences which exist show no trend with time;

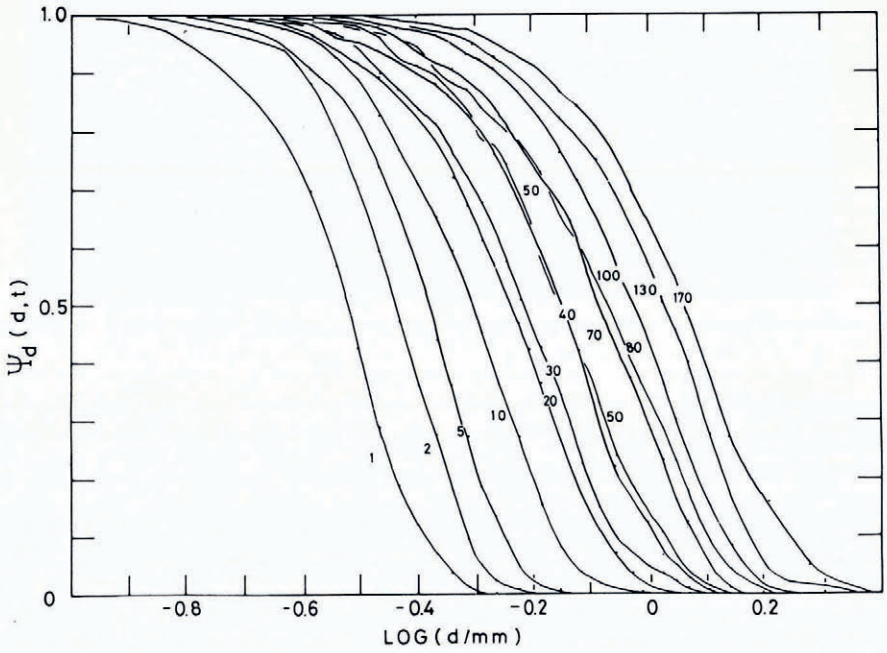

Fig. 2. Cumulative distribution of particle diameters determined for subsamples from experiment 1. See Section 2.1 for definition of Ψ_d. Numbers give time in hours after saturation.

if any trend exists, it is small and it is obscured by fluctuations in the subsamples, which probably represent statistical inhomogeneities in the sample. There is some suggestion that the distributions for 10 h and less show a slightly narrower width especially on the small-size side than the later distributions. The reader can verify these properties by shifting the curves of Figure 2 laterally for comparison.

The approximate invariance of shape on a logarithmic size scale indicates that all of the distributions shown can be approximately represented by a single distribution, which is scaled to some characteristic size. The median diameter d_m is a convenient choice, we may write

$$\Psi_d(d, t) \approx \Psi_d{}^{\star}\left(\frac{d}{d_m}\right). \tag{6}$$

Because of Equation (3) the same should hold true for $\Psi_v(v, t)$ with

$$\Psi_v(v, t) \approx \Psi_v{}^{\star}\left(\frac{v}{v_m}\right), \tag{7}$$

where

$$\Psi_v{}^{\star}\left(\frac{v}{v_m}\right) = \Psi_d{}^{\star}\left(\frac{v^{\frac{1}{3}}}{v_m{}^{\frac{1}{3}}}\right), \tag{8}$$

and v_m is median volume. This is illustrated by Figure 3, which shows the distribution v/v_m for all of the distributions shown in Figure 2. Except for some apparent deviation of the early distributions (10 h and less) and local deviations of some irregular distributions (40, 70, 80, 170 h), all of the distributions fall in a narrow band which defines $\Psi_v{}^{\star}(v/v_m)$. For either d or v a corresponding characteristic probability density distribution shapes can be defined as $\phi^{\star} = -\Psi^{\star\prime}$ so that

$$\phi_d(d, t) = \frac{1}{d_m}\phi_d{}^{\star}\left(\frac{d}{d_m}\right), \tag{9a}$$

and

$$\phi_v(v, t) = \frac{1}{v_m}\phi_v{}^{\star}\left(\frac{v}{v_m}\right). \tag{9b}$$

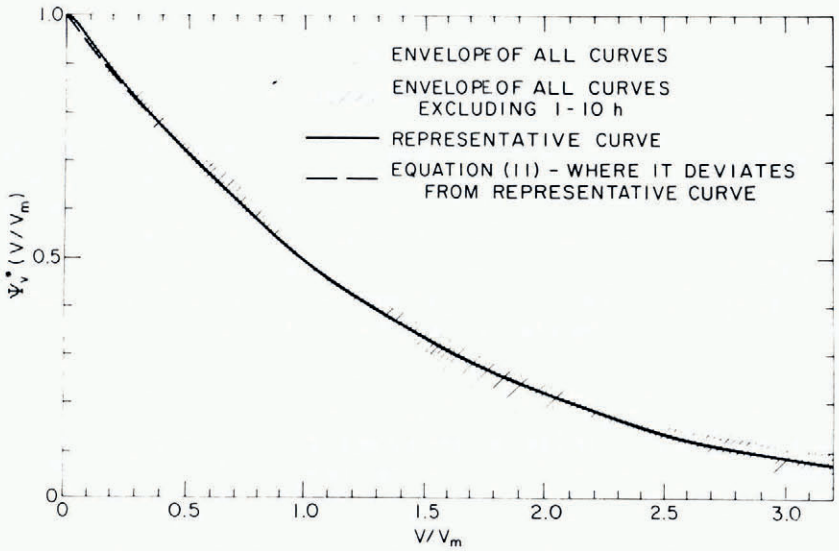

Fig. 3. Cumulative distribution of particle volumes in units of median volume for subsamples from experiment 1. See Section 2.1 for definition of $\Psi_v{}^{\star}$.

https://doi.org/10.3189/S0022143000014076 Published online by Cambridge University Press

An analytic representation of $\psi_d^\star(d/d_m)$ or $\psi_v^\star(v/v_m)$ was sought. Any logarithmic normal distribution fit to $\psi_d^\star(d/d_m)$ failed to give a good approximation to the full range of d/d_m from 0 to 2. (For example, one chosen to fit reasonably well over the range 0 to 1 diverges from the scatter band of the curves at $d/d_m = 1.1$ and predicts approximately 5% of the particles should be larger than the largest particle observed.) A normal distribution could be chosen to fall in the scatter band of the curves over nearly the full range of d/d_m, but it has the unrealistic property of giving finite probability for particles of negative size, which is very inconvenient for analysis. The best analytic representation was based on the discovery that

$$\frac{\psi_v^\star}{\phi_v^\star} \simeq b - a\left(\frac{v}{v_m}\right), \tag{10}$$

for the range of volume in which $\psi_v^\star$ is non-zero. Equations (4b) and (10) give a simple differential equation with solution

$$\psi_v^\star\left(\frac{v}{v_m}\right) \simeq \left(1 - \frac{av}{bv_m}\right)^{1/a}. \tag{11}$$

This distribution is shown on Figure 3 for $a = 0.23$ and $b = 1.55$. It agrees quite well with the measurements, except for some deviation at small sizes. It predicts zero probability for particles larger than a maximum volume of $v_m b/a = 6.8v_m$. This agrees quite well with the observed largest particle in each subsample, which had an average value of $7.6v_m$ with a standard deviation from the mean of $1.0v_m$.

A consequence of the similarity of the size distribution shapes is that there is an approximately unique relationship between median size and mean size, so

$$\bar{d}/d_m = k', \tag{12a}$$

$$\bar{v}/v_m = k, \tag{12b}$$

where $\bar{d}$ and $\bar{v}$ are mean diameter and volume. The distributions of Figure 2 give $k' = 1.013 \pm 0.009$ and $k = 1.26 \pm 0.08$. The analytic size distribution of the form given by Equations (10) and (11) has the property

$$\frac{\bar{v}}{v_m} = \frac{b}{1+a}, \tag{13}$$

which gives a value of $k = 1.26$ for the chosen values of a and b, so it fits the measured distributions reasonably well in this respect.

The details of the size distributions of subsamples in experiments other than experiment 1 were not studied. However, in all cases $\bar{d}$ and $\bar{v}$ assuming spherical shape were calculated and the relationship between them was found to be consistent with that found for the size distribution for experiment 1 shown in Figure 2. This suggests that the characteristic, nearly time-independent distribution shape found for experiment 1 and approximated by Equation (11) also describes the distributions which existed in other experiments. This has not been checked directly because of the large amount of data handling involved.

Increase of grain size with time

In all of the experiments performed, the increase in median or mean volume was found to be approximately linear with time over the time intervals studied, therefore

$$\bar{v}(t) \approx \bar{v}_0 + \bar{v}'t, \tag{14}$$

where $\bar{v}_0$ is the mean volume at $t = 0$ or time of saturation and $\bar{v}' = d\bar{v}/dt$ is a constant rate of mean volume increase.

Table II gives values of $\bar{v}_0$ and $\bar{v}'$ and their standard deviations determined by linear regression of measured mean volume of subsamples against time for experiments carried out with distilled water. The rate of mean volume change $\bar{v}'$ is essentially the same for all of these experiments.

TABLE II. RESULTS FOR DISTILLED WATER

Parameters for least-squares fit of measured $\bar{v}$ versus t to equation $\bar{v}(t) = \bar{v}'t + \bar{v}_0$.

No.	$\bar{v}' \pm \sigma(\bar{v}')$ 10^{-3} mm^3 h^{-1}	$\bar{v}_0 \pm \sigma(\bar{v}_0)$ 10^{-3} mm^3	$(r^2/n)^{\frac{1}{2}}$ 10^{-3} mm^3
1	6.0±0.2	−6±13	30
2	4.8±0.2	34±17	37
3	5.6±0.1	20± 5	8
4	6.1±0.2	8±10	18
5	5.4±0.2	30±17	36
Average	5.6±0.5		

TABLE III. RESULTS FOR SOLUTIONS

Parameters for least-squares fit of measured $\bar{v}$ versus t to equation $\bar{v}(t) = \bar{v}'t + \bar{v}_0$.

No.	*Concentration* mol/kg H_2O	$\bar{v}' \pm \sigma(\bar{v}')$ 10^{-3} mm^3 h^{-1}	$\bar{v}_0 \pm \sigma(\bar{v}_0)$ 10^{-3} mm^3	$(r^2/n)^{\frac{1}{2}}$ 10^{-3} mm^3
NaCl solution				
6	1.7×10^{-4}	5.8±0.1	−4±11	24
7	1.7×10^{-3}	5.5±0.2	10±12	28
8	0.017	5.9±0.3	−24±24	54
9	0.017	4.2±0.1	13± 9	18
10	0.1	2.7±0.1	4± 8	19
11	0.17	2.1±0.1	0± 7	16
12	1.0	0.8±0.2	9± 9	12
Glucose solution				
13	0.01	4.7±0.3	10±19	38
14	0.01	4.1±0.1	53±19	41
15	0.1	1.76±0.03	18± 2	4
16	0.1	2.5±0.1	4±10	19
17	0.1	2.5±0.2	46±43	111
18	0.5	0.62±0.02	15± 1	2
19	0.94	0.4±0.1	16±13	19
20	2.0	0.18±0.00	4± 0	1
HCl solution				
21	0.34	3.8±0.2	−5±13	22
22	0.67	1.9±0.1	−2± 4	10
Dextran solution				
23		2.5±0.1	−2± 6	15

Table III gives values of $\bar{v}_0$ and $\bar{v}'$ and their standard deviations similarly determined for experiments carried out with impure water. The rate of mean volume change is not distinguishably different from that for distilled water for low impurity concentration (less than 0.01 mol/l), but larger impurity concentrations slow the rate. The slowing of the rate by impurities can be described as

$$\bar{v}'(\text{distilled water}) = (1+f)\,\bar{v}'(\text{impure}). \qquad (15)$$

Values of f can be determined from results in Table III and a $\bar{v}'$ characteristic for distilled water from Table II. These are given in Table IV along with information about the diffusion coefficient of the impurity through water and the depression of the equilibrium temperature of the ice–solution surface caused by the impurities.

https://doi.org/10.3189/S0022143000014076 Published online by Cambridge University Press

TABLE IV. PROPERTIES OF SOLUTIONS

f Time scale parameter in Equation (15) assuming $\bar{v}' = 5.6 \times 10^{-3}$ mm³ h⁻¹ for distilled water and data from Table III.
θ Depression of ice–liquid equilibrium temperature by added impurity.
D Diffusion coefficient for impurity at 0°C.
Data for D and θ from *International critical tables* (1926–33, Vol. 4, 5).

No.	f	θ deg	D mm² s⁻¹
NaCl solution			
6	−0.03	0.000 6	0.76×10^{-3}
7	0.02	0.006 2	0.76×10^{-3}
8	−0.05	0.061	0.76×10^{-3}
9	0.33	0.061	0.76×10^{-3}
10	1.09	0.35	0.75×10^{-3}
11	1.67	0.58	0.73×10^{-3}
12	6.05	3.37	0.78×10^{-3}
Glucose solution			
13	0.19	0.019*	0.26×10^{-3}†
14	0.35	0.019	0.26×10^{-3}
15	2.18	0.19	0.26×10^{-3}
16	1.27	0.19	0.26×10^{-3}
17	1.19	0.19	0.26×10^{-3}
18	7.97	0.93	0.26×10^{-3}
19	13.46	1.75	0.26×10^{-3}
20	30.89	3.72	0.26×10^{-3}
HCl solution			
21	0.47	1.21	1.8×10^{-3}
22	2.00	2.53	2.1×10^{-3}
Dextran solution			
23	1.25	0.001 3	0.5×10^{-4}‡

* Assumes same concentration dependence as dextrose.
† Assumes concentration independent.
‡ Value for dextrin.

Figure 4 shows a master curve of all experimental results which illustrates the linearity of mean volume with time.

Equation (12b) establishes that the median volume v_m also increases linearly with time in simple proportion to $\bar{v}$. Since $\bar{v}_0$ is small, it is also found that $\bar{d}$ is approximately proportional to $t^{\frac{1}{3}}$.

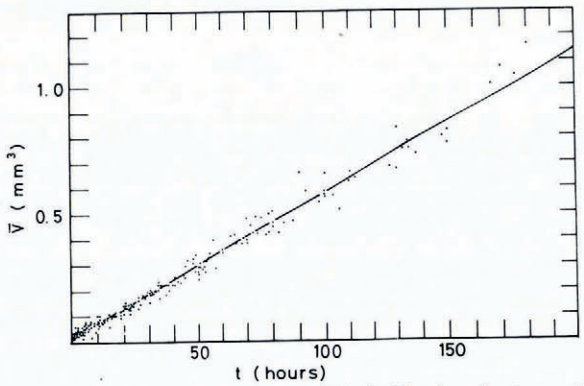

Fig. 4. Mean volume versus time for all measurements listed in Table I. The data for $\bar{v}$ versus t for any single experiment are adjusted by adding a constant to $\bar{v}$ to adjust $\bar{v}_0$ in Tables II and III to a common value of 0.020 mm³, and in the case of an experiment with impure water by scaling t by dividing by $(1+f)$ of Equation (15) with values of f from Table IV.

https://doi.org/10.3189/S0022143000014076 Published online by Cambridge University Press

2.2. *Observations of individual particles*

Experimental method

An ice cavity about 20 mm in diameter was melted in a $40 \times 40 \times 40$ mm^3 cube of ice. This ice cube was contained tightly inside of an acrylic box ($40 \times 40 \times 50$ mm^3) which was held in place inside of a larger acrylic box ($70 \times 70 \times 62$ mm^3). Ice plates were placed in the gaps between the walls of the boxes. The ice was coarsely crystalline, bubble-free ice (grain size *c.* 20 mm) grown from de-ionized water, or in some cases cut from single crystals of Mendenhall Glacier ice. Before assembly all plastic and ice pieces were thoroughly rinsed in distilled water. Once assembled, all void spaces in the apparatus were filled with distilled, de-ionized water. The outer box was surrounded by styrofoam insulation thickness of *c.* 10 mm. The apparatus was used in a cold room at (0.0 ± 0.2)°C.

The cavity was used for two types of experiments. In the first, particles were introduced into the cavity through an access tube leading to a hole in the base of the cavity. The particles would float upward into the cavity and were caught and held in the center of the cavity by a domed polyethelene membrane of 0.03 mm thickness (Fig. 5a). Such particles interacted with the walls of the cavity only through the intervening water mass. This experiment allows observation of volume change in an isolated small ice particle immersed in water in which the initial temperature is equal to the equilibrium temperature of the nearly planar walls of the

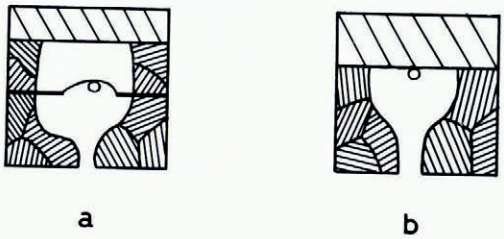

Fig. 5. Configuration of ice cavity and ice particles for two types of experiments for measurements of single particles.

cavity. In the second type of experiment, particles were introduced in a similar way, but allowed to float upward to contact the planar surface of a single-crystal plate of ice. Alternatively particles were allowed to bond to a single-crystal plate and this was then used to construct the roof of the cavity (Fig. 5b). This experiment allows observation of the effect of a direct mechanical contact between surfaces of different curvature. The first type of experiment has the advantage that it can be analyzed precisely (Section 4.2). The second type is more directly relevant to grain growth in snow because it models the situation of a small particle in contact with a large particle, which is the probable situation of most small particles in the bulk snow in the last stages of their existence. Groups of particles were also introduced into the cavity and the shrinkage of small particles surrounded by various configurations of other particles could be observed.

Change of particle size with time was observed using a 16 mm time-lapse movie camera looking vertically downward. A 45 mm lens was positioned to give an image magnification of 4.5. Illumination was from a tungsten lamp with total unfiltered beam intensity of about 8×10^{-4} W/mm^2 at the sample. The beam was filtered using a polarizer, a heat filter, and 0.2 m of iced water to remove spectral components which could be absorbed by the water of the cavity. The lamp was on for only 1 s at the time of each exposure, which were spaced every 60 to 240 s. Radiation absorbed in the cavity was negligible under these conditions.

Measurement of the images was made by projection onto an analyzer screen giving a total magnification of projected size to real size of 103 to 104. Diameter of the image could be measured with an accuracy of about 1 mm. This gives an accuracy at the real scale of ± 0.01 mm and corresponds to an error in volume determination of ± 0.02 mm $v^{\frac{2}{3}}$.

Summary of results

Observations were made of particles with the configurations of Figures 5a and b, and also particles in undefined configurations of surrounding particles achieved in the above experiments and the time-lapse movie of Wakahama (1975). Each of these particles showed an approximately linear volume decrease with time. For an individual particle, root-mean-square deviation of data points from a least-squares fit straight line was in the range of $(0.03$ to $1.14) \times 10^{-3}$ mm^3 for initial volumes in the range $(0.6$ to $36) \times 10^{-3}$ mm^3 which is compatible with the errors of volume determination. The rates of volume change are summarized in Table V. Particles in the same situation showed fairly consistent rates of change except for two anomalous particles which showed exceptionally large deviations from the typical rate.

TABLE V. RATE OF VOLUME DECREASE OF INDIVIDUAL SMALL PARTICLES

Units of 10^{-3} mm^3 h^{-1}

Configuration	*No. observed*	*Average rate*	*Minimum rate*	*Maximum rate*
Figure 5a	6	4.0 ± 1.6*	1.6	11.7† (5.2*)
Figure 5b	6	10.0 ± 2.5*	5.8	38.2† (12.5*)
In group of larger particles	19	7.3 ± 2.7	3.0	13.6

* Excluding one anomalous particle.
† Considered anomalous, number in brackets gives maximum rate excluding anomalous particle.

3. ANALYSIS OF EXPERIMENTAL DATA

In this section we analyze the size distributions of particles in bulk snow experiments in order to determine the behavior of typical particles. This is compared to the available direct observations of single particles.

To start, we consider a reference volume v for which the total number of particles larger than or equal to v is constant with time. This can be expressed as

$$\mathcal{N}(t)\Psi_v(v, t) = \mathcal{N}(t_0)\Psi_v(v_0, t_0), \tag{16}$$

where the right-hand side is the total number of particles larger than or equal to v_0 at reference time t_0 and v is chosen in the left-hand side so that the total number of particles larger than or equal to v is the same as for v_0 at t_0. Equation (16) defines a trajectory of reference volume versus time which passes through (v_0, t_0) and is associated with a specific value of $\mathcal{N}\Psi_v$. The total differential of the left-hand side of Equation (16) is zero, which gives the differential form

$$\frac{\partial \Psi_v(v, t)}{\partial t} = -S(v, t)\frac{\partial \Psi_v(v, t)}{\partial v} - \frac{\Psi_v(v, t)}{\mathcal{N}(t)}\frac{\mathrm{d}\mathcal{N}(t)}{\mathrm{d}t}, \tag{17}$$

where

$$S(v, t) = \partial v/\partial t, \tag{18}$$

represents the slope of the trajectory.

https://doi.org/10.3189/S0022143000014076 Published online by Cambridge University Press

The trajectories of constant $N\Psi_v$ can be defined without reference to any particular process causing the size distribution changes; they simply provide another way of describing the changes. We make the hypothesis that the number of particles larger than or equal in size to a given particle is approximately constant. This is consistent with the observations of sample evolution presented in Section 2.1 in which small particles decrease in size and large ones increase in size. The number would be precisely constant, if for an arbitrary pair of particles v_1 and v_2, $v_1 > v_2$ implies $dv_1/dt > dv_2/dt$. In this case the trajectories of reference volume would precisely parallel trajectories of actual individual particles. In actuality, the hypothesis is likely to be true only in the approximate form stated, in which case the trajectories parallel "typical" particles or statistical particles.

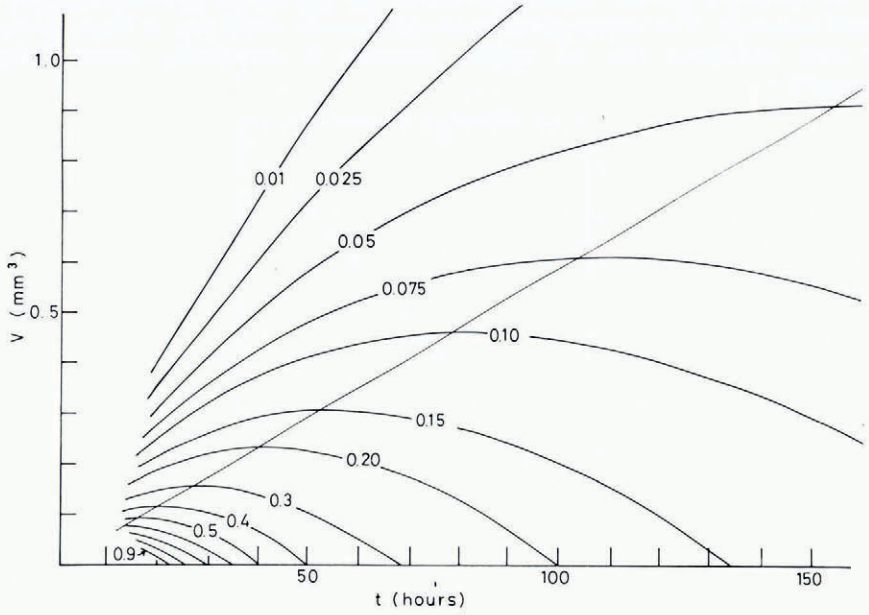

Fig. 6. Statistical particle trajectories deduced for experiment 1 from Equation (19). Numbers on curves give value of Ψ_v *at a reference time of 20 h.*

The simple relationship between size distributions at different times expressed by Equation (7) facilitates calculation of the trajectories from Equation (16). Substitution gives

$$v(t) = v_m(t)\Psi_v{}^{\star-1}\left[\frac{v_m(t)}{v_m(t_0)}\,\Psi_v{}^{\star}\left(\frac{v(t_0)}{v_m(t_0)}\right)\right], \tag{19}$$

and this gives the results shown in Figure 6. When Equations (2), (12b), and (7) are substituted into Equation (17), one finds

$$S_v(v,t) = \frac{dv_m}{dt}\left[\frac{v}{v_m} - \frac{\Psi_v{}^{\star}(v/v_m)}{\phi_v{}^{\star}(v/v_m)}\right]. \tag{20}$$

Since $dv_m/dt = v_m'$ is constant, this last equation shows

$$S_v(v,t) = S_v{}^{\star}\left(\frac{v}{v_m}\right), \tag{21}$$

https://doi.org/10.3189/S0022143000014076 Published online by Cambridge University Press

that is the rate of volume change of a statistical particle depends only on the ratio v/v_m independent of time. This fact is visible in Figure 6, where the slopes of particle trajectories are constant along straight lines drawn through the origin any one of which has the approximate interpretation $v = kv_m$, k constant.

Figure 7 shows $S^\star(v/v_m)$ deduced from Equation (20) and the measured size distribution (Fig. 3). It turns out to be approximately linear. The boundary between small shrinking particles and large growing particles is given by that volume for which $S^\star(v/v_m) = 0$, and this turns out to be $v = 1.26v_m$, which from Equation (12b) is approximately the mean volume $\bar{v}$. $S^\star(0)$ has the value of about -9×10^{-3} mm^3 h^{-1}. This agrees quite well with the rates of volume change given in Table V for particles in the configuration of Figure 5b, which should match the local environment of a very small particle in saturated snow. Therefore, we find that the statistical particle trajectories match the trajectories of individual particles at least at small volumes. The largest particles at any time are about $7v_m$ as discussed in Section 2.1 and their predicted rate of volume increase is necessarily about $7\,dv_m/dt$ or 31×10^{-3} mm^3 h^{-1}.

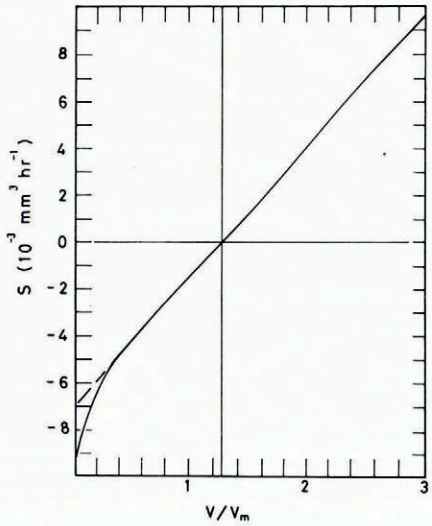

Fig. 7. Rates of volume change of statistical particles deduced from Equation (20). Solid curve is deduced from representative curve of Figure 3; dashed curve is deduced from Equation (11), which corresponds to the dashed curve in Figure 3.

If the distribution of particle sizes were given by Equation (11) with the properties described by Equations (10) and (13), then Equation (20) would give

$$S^\star\left(\frac{v}{v_m}\right) = S_0\left[\frac{v}{\bar{v}} - 1\right], \tag{22}$$

where

$$S_0 = b\,dv_m/dt.$$

This perfectly linear description of $S^\star(v/v_m)$ is indistinguishable from that determined from the measured distribution except possibly at very small volumes.

4. Physical model of grain coarsening

It has been proposed that grain coarsening in saturated snow is determined by the effect of curvature of an ice–water interface on its temperature (Wakahama, 1968; Colbeck, [1975]).

https://doi.org/10.3189/S0022143000014076 Published online by Cambridge University Press

This effect causes small particles to be colder than large particles with the result that the small ones melt and the large ones freeze. Qualitatively this seems to fit earlier observations (Wakahama, 1968, [1975]) and the ones presented here. Another possible mechanism would be mass transfer directly through the solid phase by volume diffusion, but the very slow rates of texture change when the void space is occupied by air or kerosene show this process is too slow to be significant in the rapid changes of water-saturated snow (Hobbs and Mason, 1964). In this section we develop the model of melting and freezing to give quantitative predictions of various aspects of our observations.

4.1. *Foundations*

(i) Melting or freezing at an interface is caused by a net heat flow to or from the interface. If n is measured along a coordinate axis pointing normally outward from an ice-particle surface, then this may be expressed as

$$\frac{\mathrm{d}n}{\mathrm{d}t} = -\frac{q_\mathrm{w}+q_\mathrm{i}}{\rho_\mathrm{i}h}, \tag{23}$$

where the heat flowing to the interface from the water is q_w and from the ice is q_i, and where ρ_i is the density of ice and h is the latent heat of fusion per unit mass. The heat flux from the water can be expressed as

$$q_\mathrm{w} = K_\mathrm{w}\frac{\partial T}{\partial n}, \tag{24}$$

where K_w is the thermal conductivity of the water. We could also relate q_i to the conductivity and temperature gradient in the ice, but it is convenient to express it as a fraction of the flux from the water. Equations (23) and (24) give

$$\frac{\partial T}{\partial n} = -\frac{\rho_\mathrm{i}h}{K_\mathrm{w}}\frac{1}{(1+q_\mathrm{i}/q_\mathrm{w})}\frac{\mathrm{d}n}{\mathrm{d}t}, \tag{25}$$

where the surface-normal derivative of temperature refers specifically to the liquid side of the interface.

(ii) Most impurities have extremely low solubility in solid ice (Paren and Walker, 1971). For practical purposes it can be assumed that all impurities are excluded from the ice and are dissolved in the liquid. As a result there must be some transport of impurities by diffusion near a melting or freezing interface. The impurity flux density outward across a surface fixed in the liquid infinitesimally close to the solid liquid interface is $-D\,\partial(\rho_\mathrm{w}c)/\partial n$, where D is the diffusion coefficient for the solute, c is the amount of solute per unit water mass, and ρ_w is water density. The solute excluded from the advancing solid interface gives an effective rate of solute production per unit area of $(\rho_\mathrm{w}c)\times(\mathrm{d}n/\mathrm{d}t)(\rho_\mathrm{w}/\rho_\mathrm{i})$, where the first part is the amount of solute per unit water volume and the second is the rate at which water volume is frozen on to the advancing interface. The outward flux and production rates must balance, which gives

$$\frac{\partial c}{\partial n} = -\frac{\rho_\mathrm{i}c}{\rho_\mathrm{w}D}\frac{\mathrm{d}n}{\mathrm{d}t}, \tag{26}$$

where the normal derivative again refers to the liquid side of the interface.

(iii) For analysis we will assume that there is no motion of the water. This is probably true to a high degree in most of the experiments. Water circulation was forced in experiments 4 and 5, but in these cases there was no noticeable effect on the experimental results. Apparently the water motions can be neglected, but that might not be the case for natural conditions. Without water motion the transport of heat and solute is by diffusion alone, and their distributions can be found from appropriate diffusion equations. Furthermore, they

can be determined from the time-independent diffusion equation (Laplace's equation). This can be tested by comparing the time scale to eliminate transients from the distributions with the time over which there is significant change in the configuration of the solid–liquid interfaces and the corresponding boundary conditions determined by the configuration. Transients in the temperature field are eliminated on a time scale of

$$t_T^{\star} \approx \frac{d^2}{\pi^2 \kappa}, \tag{27}$$

where d is on the order of the dimensions of the particles and the gaps between, and κ is thermal diffusivity (see Carslaw and Jaeger, 1959, section 1.3). For solute concentration, the corresponding time scale is

$$t_c^{\star} \approx \frac{d^2}{\pi^2 D}, \tag{28}$$

where D is diffusion coefficient. The time needed for significant change in geometry can be estimated as

$$t_g^{\star} \approx \frac{d}{\mathrm{d}n/\mathrm{d}t}. \tag{29}$$

With $d \approx 0.5$ mm, $\mathrm{d}n/\mathrm{d}t \approx 10^{-5}$ mm s^{-1} from experiment, $K = 0.1$ mm^2 s^{-1}, and $D = 0.2 \times 10^{-2}$ mm^2 s^{-1}, we find $t_T^{\star} \approx 0.2$ s and $t_c^{\star} \approx 13$ s, which are both less than $t_g^{\star} \approx 5 \times 10^4$ s. Therefore, transients are eliminated faster than boundary conditions change and the temperature and solute concentration fields are effectively steady.

(iv) The local temperature at a point on a solid–liquid interface is given by

$$T = \delta - \beta p - 2\alpha\chi - \zeta c, \tag{30}$$

where $\delta = 0.010\ 0$°C ≈ 273.16 K is the triple-point temperature, β is the Clausius–Clapyron slope giving the effect of pressure p, α expresses the effect of average interface curvature χ (χ being positive when surface is convex toward liquid), and ζ expresses the effect of impurities depending on the solution concentration c expressed in molality. With gas constant $R = 4.62 \times 10^2$ J deg^{-1} kg^{-1}, $T = \delta$ in kelvins, solid–liquid interface energy $\gamma_{SL} = 0.034$ J m^{-2}, heat of fusion $h = 3.34 \times 10^5$ J kg^{-1}, ice density $\rho_i = 0.92$ Mg m^{-3}, water density $\rho_w = 1.00$ Mg m^{-3}, and molar weight of $H_2O = 18$ g, standard thermodynamical relationships give numerical values $\beta = (1/\rho_i - 1/\rho_w)\, T/h = 0.007\ 4$ deg bar^{-1}, $\alpha = T\gamma_{SL}/h\rho_i = 3.02 \times 10^{-8}$ deg m, and $\zeta = (RT^2/h)(M_w/1\ 000) = 1.86$ deg mol^{-1} kg. The quantity ζ must be corrected when the solute dissociates or the solution is non-ideal and in these circumstances it depends somewhat on concentration; these factors are important for some of the entries in column 3 of Table IV.

Equation (30) includes a number of implicit physical assumptions and mathematical approximations. First it assumes equilibrium of the interface. Experimentally the rates of freezing are on the order of 10^{-6} mm s^{-1}, which give interface supercooling of the order of 10^{-4} deg or less (Fletcher, 1970, p. 115). Although not necessarily negligible, this is small in comparison with the terms of interest in Equation (30), where temperature deviations from surface curvature of typical particles (diameter 1 mm or less) are 10^{-4} deg or more and from impurities are 10^{-3} deg or more. Also validity of Equation (30) requires that temperature deviates only slightly from the triple point ($|\delta - T|/T \ll 1$) and that the liquid phase be a dilute solution ($cM_w/1\ 000 \ll 1$), both of which are satisfied quite well for the conditions considered here. Also we use Equation (30) assuming α is independent of c and χ, and ζ is independent of χ for which there is theoretical justification (Dufour and Defay, 1963, p. 59–64).

4.2. *Effect of impurities*

Most of the experiments used distilled water and melt water in natural snow can be very pure. Nevertheless, in the experiments and in Nature the liquid is probably nearly saturated with respect to atmospheric air, which causes a temperature depression of about 0.002 deg. This is substantial in comparison with the temperature effect of particle surface curvature, so the consequences of impurities must be considered for all of the experiments.

The qualitative effect of impurities is to slow the process of texture change. The solute concentration tends to be low at places of melting because of dilution by the melt water and tends to be high at places of freezing because of concentration by exclusion from the advancing solid phase. The result is to lower the temperature differences caused by differences in particle surface curvature.

In order to study the quantitative effect of impurities, we use the fact that the distributions of temperature and solute are both governed by Laplace's equation and similar boundary conditions. Although it is impractical to establish exactly what the distributions are, a certain simple relationship between them can be established. This relationship can be used to determine how much a given amount of impurity slows metamorphism of the snow in comparison with pure conditions.

To start we make two approximations. The first is that q_i/q_w in Equation (25) is independent of position on the solid–liquid interface. This may not be very precise, but we can hope that some average value of q_i/q_w may reasonably characterize all locations on the solid–liquid interfaces. Equation (25) then may be written as

$$\frac{\partial T}{\partial n} = -k_T \frac{\mathrm{d}n}{\mathrm{d}t}, \tag{31a}$$

where

$$k_T = \frac{\rho_i h}{K_w} \frac{1}{(1+q_i/q_w)}, \tag{31b}$$

is a "constant". The second approximation concerns Equation (26). From it and the expectation that the largest gradients in c are at the melting and freezing interfaces, we can conclude

$$\frac{|\bar{c}-c|}{d} < \frac{\rho_i c}{\rho_w D} \left|\frac{\mathrm{d}n}{\mathrm{d}t}\right|, \tag{32}$$

where d is of the order of the dimensions of the liquid pods between the grains and $\bar{c}$ is the average solute concentration. Since $d \approx 0.5$ mm, $|\mathrm{d}n/\mathrm{d}t| \approx 10^{-5}$ mm s^{-1} and $D \approx 0.2 \times 10^{-2}$ mm^2 s^{-1}, $|\bar{c}-c|/c < 2 \times 10^{-3}$. For this reason we may replace c evaluated at the interface on the right-hand side of Equation (26) with $\bar{c}$, the average value. This introduces negligible fractional error and then

$$\frac{\partial c}{\partial n} = -k_c \frac{\mathrm{d}n}{\mathrm{d}t}, \tag{33a}$$

where

$$k_c = \frac{\rho_i \bar{c}}{\rho_w D}, \tag{33b}$$

is a constant. With these approximations $\partial T/\partial n$ and $\partial c/\partial n$ are both proportional to $\mathrm{d}n/\mathrm{d}t$.

Now consider a case of grain coarsening where the liquid contains impurities. There is some definite arrangement of the solid–liquid interfaces and some definite distribution of

https://doi.org/10.3189/S0022143000014076 Published online by Cambridge University Press

dn/dt on these surfaces. Let Φ be a solution to Laplace's equation defined throughout the liquid subject to the boundary condition

$$\frac{\partial \Phi}{\partial n} = 1 \times \frac{dn}{dt}, \tag{34}$$

on the solid–liquid interfaces. The normal derivative boundary condition determines Φ only to within an additive constant; we specify Φ uniquely by requiring in addition that its average throughout the water be zero. The distributions of T and c can be written in terms of Φ as

$$T(\mathbf{x}) = -k_T \Phi(\mathbf{x}) + \bar{T}, \tag{35a}$$

$$c(\mathbf{x}) = -k_s \Phi(\mathbf{x}) + \bar{c}, \tag{35b}$$

where $\bar{T}$ and $\bar{c}$ are the respective average values of T and c in the liquid and $\mathbf{x}$ is position vector. These satisfy Laplace's equation and the boundary conditions of Equations (31) and (33).

In the above case the temperature depression at a location $\mathbf{x}_s$ on a liquid–solid interface caused by impurities is $\zeta c(\mathbf{x}_s)$ from Equation (30). If these impurities were absent and the conditions of pressure and interface curvature were the same; the temperature of the interfaces would be

$$T_{\text{pure}}(\mathbf{x}) = T(\mathbf{x}) + \zeta c(\mathbf{x}) = -(k_t + \zeta k_s)\, \phi(\mathbf{x}) + \bar{T} + \zeta \bar{c}, \tag{36}$$

where $\mathbf{x}$ lies on the interface. This gives a boundary condition, which can be used to determine the temperature distribution for the case that impurities are absent in terms of the case that they are present. Indeed we see that Equation (36) gives that distribution when we allow $\mathbf{x}$ to be any position in the liquid; it satisfies the boundary condition and Laplace's equation.

Equations (31) can be used to compute dn/dt from the temperature gradient normal to the interface. For the case of impure water we find from Equation (35a) that

$$\frac{dn}{dt} = -\frac{1}{k_T} \frac{\partial T}{\partial n}(\mathbf{x}_s) = \frac{\partial \Phi}{\partial n}(\mathbf{x}_s), \tag{37}$$

which comes from the original definition of Φ. For the case of pure water we find from Equation (36)

$$\left.\frac{dn}{dt}\right|_{\text{pure}} = -\frac{1}{k_T} \frac{\partial T}{\partial n}(\mathbf{x}_s) = \left(1 + \frac{\zeta k_c}{k_T}\right) \frac{\partial \Phi}{\partial n}(\mathbf{x}_s). \tag{38}$$

Comparison of Equations (37) and (38) shows

$$\left.\frac{dn}{dt}\right|_{\text{pure}} = (1+f) \left.\frac{dn}{dt}\right|_{\text{impure}}, \tag{39a}$$

where

$$f = \frac{\zeta k_c}{k_T} = (1 + q_i/q_w) \frac{K_w \theta}{\rho_w h D}, \tag{39b}$$

with $\theta = \zeta \bar{c}$ being the temperature depression associated with the average impurity concentration.

To test this theory, values of f determined from the experiments (Table IV) are plotted in Figure 8 against $K_w \theta / \rho_w h D$ using available values of diffusion coefficient. The experimental results for all of the tested solutions are in good agreement with the theory if $q_i/q_w \approx 0.23$. Apparently most of the heat in the melting and refreezing mechanism is conducted through the liquid phase.

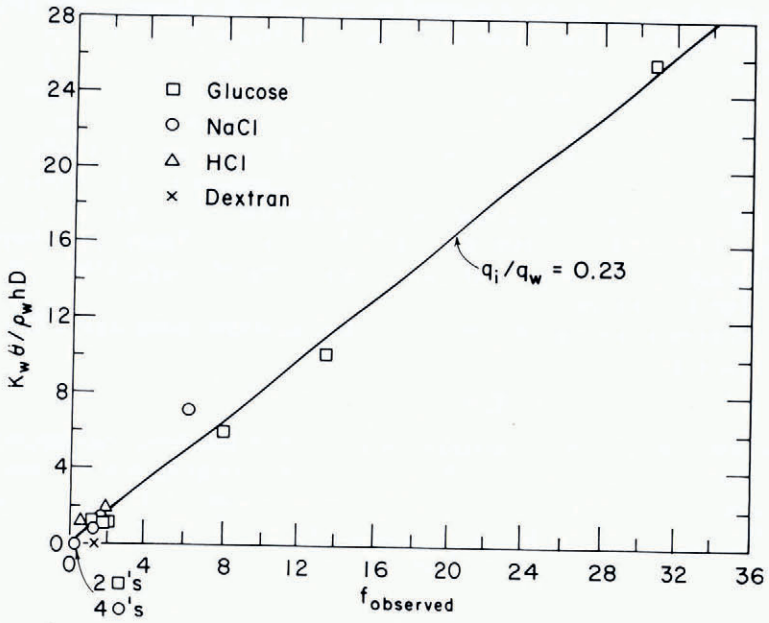

Fig. 8. Comparison of time-scaling parameter f in Equation (15) observed experimentally and predicted theoretically from Equation (39b). Straight line corresponds to a value of $q_i/q_w = 0.23$ in Equation (39b).

4.3. *Theoretical melting rate of small particles*

It is possible to make a rough estimate of how fast very small particles should melt from the model of Section 4.1. This is worked out for pure water in this section. The effect of impurities can be found from the results of Section 4.2.

A simple analysis can be based on a model that the small ice particle is in the central part of a liquid cavity between much larger surrounding particles. Carslaw and Jaeger (1959, p. 247) give the solution for temperature around a sphere of temperature T_0 immersed in an initially isothermal infinite medium of temperature T_w. After a time $t_T{}^\star$ given by Equation (27) of seconds or less, a time-independent temperature gradient is set up at the particle surface of

$$\frac{\partial T}{\partial n} = -\frac{2(T_0 - T_w)}{d}. \tag{40}$$

The temperature difference between the small particle and the surrounding liquid or other particles is dominated by the large curvature ($\chi = 2/d$) of the small particle, so from Equation (30) we expect

$$T_w - T_0 \approx 4\alpha/d. \tag{41}$$

Furthermore in this case there is no flow of heat in the ice particle ($q_i = 0$). From Equations (25), (40), and (41), we find

$$\frac{dv}{dt} = -\pi d^2 \frac{dn}{dt} = -\frac{8\pi K_w \alpha}{\rho_i h} = -4.9 \times 10^{-3}\ \text{mm}^3\ \text{h}^{-1}. \tag{42}$$

This is in excellent agreement with the rates of volume decrease observed for isolated particles of $(4.0 \pm 1.6) \times 10^{-3}$ mm^3 h^{-1} (Table V).

https://doi.org/10.3189/S0022143000014076 Published online by Cambridge University Press

In snow a small particle is not suspended in the center of a liquid pocket but floats to the top of the pocket to contact one or two of the bounding larger particles. The proximity of the small particle to a low-curvature surface and conduction through the solid should increase the melting rate to be somewhat larger than given by Equation (42). A precise calculation is difficult, since the small particle is to some extent deposited locally on the contacting large particle, so there is a lump and a correspondingly complex distribution of surface temperature. However, the increase by roughly a factor of two suggested by the experiments (Fig. 5, Table V) is very reasonable. Therefore, we conclude that the values of $(10.0 \pm 2.5) \times 10^{-3}$ $mm^3\ h^{-1}$ observed directly (Section 2.2) and of *c.* $8\text{–}9 \times 10^{-3}\ mm^3\ h^{-1}$ inferred from size distribution changes (Sections 3.1 and 3.2) are quantitatively compatible with the physical model of melting and freezing.

Since the local environment of a very small particle in saturated snow is likely to be fairly unique, we expect that

$$S_0 \approx 1 \times 10^{-2}\ mm^3\ h^{-1}, \tag{43}$$

characterizes the rate of volume decrease of very small particles independent of the size distribution of the particular sample of snow. This expectation is confirmed by the good agreement between the experimental rates of volume decrease deduced for small particles in bulk snow (Fig. 7), particles of configuration in Figure 5b (Table V, row 2), and small particles in groups of larger particles (Table V, row 3).

4.4. *Explanation of linear increase of mean volume*

When Equation (18) is evaluated for $v = 0$, it gives

$$\frac{1}{\mathcal{N}(t)} \frac{d\mathcal{N}(t)}{dt} = -S(0, t) \frac{\partial \Psi}{\partial v}(0, t) = S(0, t)\, \phi_v(0, t), \tag{44}$$

which is simply a statement that the total number of particles decreases at a rate equal to the number of very small particles per unit volume interval times the rate at which these small particles lose volume. From Section 4.3, we expect $S(0, t) = -S_0$ where S_0 is a constant independent of the size distribution. When this is combined with conservation of the total ice volume expressed by Equation (2), we find

$$\frac{d\bar{v}}{dt} = S_0 \bar{v} \phi_v(0, t). \tag{45}$$

If it arises that the size distribution establishes any stable time-independent shape as expressed in Equation (7) or equivalently (9b), then

$$\frac{d\bar{v}}{dt} = S_0 \phi_v^{\star}(0)\, k, \tag{46}$$

where $k = \bar{v}/v_m$ is a constant. Thus $d\bar{v}/dt$ is independent of time. Notice that this fact does not depend on the size distribution establishing any specific special shape, only that it reaches any steady shape. This behavior therefore probably depends only on very general aspects of the physical mechanism of grain coarsening, which allows the particle size distribution to evolve into a steady shape.

To predict the quantitative value of $d\bar{v}/dt$, it is necessary to predict the shape of the size distribution, so $\phi_v^{\star}(0)$ and k can be found. Equation (21) shows that once a steady shape has been reached, $S(v, t)$ is zero for that volume particle such that

$$0 = \frac{v}{v_m} - \frac{\Psi_v^{\star}(v/v_m)}{\phi_v^{\star}(v/v_m)}. \tag{47}$$

Without concerning ourselves about the details of the physics, we can probably safely assume that particles of about median or mean size are neither shrinking or growing on the average. In other words Equation (47) should hold roughly when $v = v_m$. Since $\Psi_v^\star(1) = 0.5$ by definition, this gives

$$\phi_v^\star(1) = 0.5. \tag{48}$$

Now the average value of $\phi_v^\star(v/v_m)$ between 0 and 1 is

$$\left\langle \phi_v^\star\left(\frac{v}{v_m}\right)\right\rangle_0^1 = (\Psi_v^\star(0) - \Psi_v^\star(1))/1.0 = 0.5. \tag{49}$$

The equality of $\phi_v^\star(1)$ and its average value between 0 and 1 suggests that $\phi_v^\star$ must have a fairly constant value of about 0.5 between 0 and 1, so that

$$\phi_v^\star(0) \approx 0.5. \tag{50}$$

Now in actuality $S(v, t)$ may not be precisely zero for median size. In fact in the experiments it is zero for a size more closely equal to the mean volume, and the value of $\phi_v^\star(v/v_m)$ shows some variation in the range of about 0.6 to 0.4 over the interval of v/v_m from 0 to 1. Nevertheless, the above argument provides a good approximation and predicts that $\partial\bar{v}/\partial t$ should be roughly half of S_0 which is in good accord with the experimental results, where $\partial\bar{v}/\partial t = (5.6 \pm 0.5) \times 10^{-3}$ mm^3 h^{-1} and $S_0 = (10.0 \pm 2.5) \times 10^{-3}$ mm^3 h^{-1}.

5. Discussion

An important and basic question concerns the explanation of why the size distributions reach a final steady shape described by Equation (7), in which a unique shape is scaled to a characteristic volume. Intuitively this behavior is reasonable. The basic process in which particles get bigger by other particles getting smaller leads to an increase in spread of the size distribution with time. If small particles could shrink indefinitely without disappearing, the mean volume would remain constant and the spread of particle size would increase with time. However, once some particles reach the boundary of zero volume, the spread tends to be determined by the mean size, and the mean size starts to increase. It is reasonable that subsequently the smaller particles are distributed between the mean size and zero volume in some characteristic fashion. This would tend to give behavior like that described in Equation (7). This behavior is determined by conservation of volume and the boundary of zero volume.

A related question concerns the actual final shape, which for a sample initially composed of new dry snow is shown in Figure 4. For example, would the same final shape be reached if the initial size distribution were substantially different, or is the apparent final shape in fact evolving at a slow but unobservable rate? These questions are important in order to understand what might happen in different snow or on a time scale much longer than in the experiments. Based on the assumption that the rate of volume change of particles of approximately median volume is zero, the argument in Section 4.4 suggests that the slope of $\Psi_v^\star(v/v_m)$ must have a fairly uniform slope of about 0.5 between $v = 0$ and $v = v_m$, but this is only a semiquantitative conclusion.

If the rate of volume change of particles $S(v, t)$ could be predicted for any arbitrary size distribution, then Equation (17) could be used to give a rigorous and quantitative calculation of the changes of size distribution with time. In principle, the rate of volume change of each particle in any specific sample could be determined based on the physical foundations given in Section 4.1. The temperature of particle surfaces is given by Equation (30). The resulting heat flow is quasi-steady so that the source of heat arriving at a location on one particle surface may be traced uniquely to the surface of another particle. This means one can speak of thermal contact between particles with well-defined reciprocal heat exchange and corresponding ice-mass exchange between them. A starting point is to analyse the heat exchange

between particle pairs based on the temperature difference and the thermal resistance between them, as was attempted by Colbeck ([1975]). However, a practical and useful theoretical prediction of $S(v, t)$ must have a primarily statistical element to it. The relationship between particle surface temperature and particle volume and the thermal resistance between thermally contacting particles cannot be uniquely related to the particle sizes because of variations in particle shape and arrangements.

Greenwood (1956) has considered the growth rates of dispersed particle precipitates in solutions. This process is called Ostwald ripening. The diffusion of solutes controlled by particle surface curvature is analogous to the diffusion of heat in the grain growth of wet snow. He predicts that the rate of change of particle volume depends linearly on particle diameter and is zero for mean diameter particles. This is different from the results of our experiments which show that $S(v, t)$ varies linearly with particle volume and is zero for mean volume particles (Fig. 7). Lifshits and Slyozov (1961) have considered the same problem starting that they are present. Indeed we see that Equation (36) gives that distribution when we allow with essentially the same form of $S(v, t)$ as derived by Greenwood to deduce asymptotic particle-size distribution shapes, but because that form is not applicable to our experiments, their predictions are also at variance with the steady distribution shapes we observed. They predict maximum-size particles with diameter 1.5, or volume 3.4, times the particle size which is instantaneously neither shrinking nor growing, but we find maximum-size particles substantially larger than this. These treatments deal with dispersed particles in which particles interact with the solution in a locally spherically symmetric environment but only indirectly with one another. In this case $S(v, t)$ can be expressed independently of the details of particle-size distribution shape, and makes a relatively simple analysis possible. The partial failure of the treatments probably hinges on the close packing of the ice particles in snow and the importance of direct particle-to-particle interactions and the consequent statistical problems.

6. Summary

The basic features of the changes that take place in water-saturated snow can be explained in terms of heat-flow controlled melting and refreezing determined by the curvature of particle surfaces. The melting rate of small particles predicted theoretically is in good quantitative agreement with observation. This melting rate is expected to be independent of the size distribution (Section 4.3). Once the size distribution establishes an asymptotic steady shape, the subsequent constant rate of increase of mean volume is a consequence of volume conservation. The expectation that particles of roughly median size will be at the boundary between smaller particles which are shrinking and larger particles which are growing leads to the conclusion that the established steady shape of the cumulative distribution of particle volumes has a relatively uniform slope between zero and median size and that the actual rate of increase of mean volume is roughly one-half the melting rate of small particles, in good agreement with observation (Section 4.4). The observed effect of impurities can be explained quantitatively in terms of their effect on melting temperature, exclusion from the solid phase, and diffusion through the liquid phase. Natural amounts of impurity in snow have negligible effect. The effect of larger amounts indicate that heat flow in the melting–freezing process of grain growth occurs primarily through the liquid phase, but about 19% of the heat transport to or from particle surfaces occurs through the ice (Section 4.2).

Acknowledgements

We wish gratefully to acknowledge the continuous encouragement given to us by Professor G. Wakahama, whose pioneering studies of wet-snow metamorphism formed the foundation for this work. One of us wishes to express thanks to the University of Washington, which

granted a sabbatical leave to permit his participation in this work, and also to the director, Professor D. Kuroiwa, and the staff of the Low Temperature Institute of Hokkaido University for their tremendous hospitality.

MS. received 8 February 1978 and in revised form 26 April 1978

REFERENCES

Anderson, D. L., *and* Benson, C. S. 1963. The densification and diagenesis of snow. (*In* Kingery, W. D., *ed. Ice and snow; properties, processes, and applications: proceedings of a conference held at the Massachusetts Institute of Technology, February 12–16, 1962.* Cambridge, Mass., M.I.T. Press, p. 391–411.)

Carslaw, H. S., *and* Jaeger, J. C. 1959. *Conduction of heat in solids. Second edition.* Oxford, Clarendon Press.

Chai, B. H. T. [c1974.] Mass transfer of calcite during hydrothermal recrystallization. (*In* Hofmann, A. W., *and others, ed. Geochemical transport and kinetics. Papers presented at a conference at Airlie House, Warrenton, Virginia, June 1973. Edited by A. W. Hofmann, B. J. Giletti, H. S. Yoder, Jr., and R. A. Yund.* [Washington, D.C.,] Carnegie Institution of Washington, p. 205–18. (Carnegie Institution of Washington Publication No. 634.))

Colbeck, S. C. 1972. A theory of water percolation in snow. *Journal of Glaciology*, Vol. 11, No. 63, p. 369–85.

Colbeck, S. C. [1975.] Grain and bond growth in wet snow. [*Union Géodésique et Géophysique Internationale. Association Internationale des Sciences Hydrologiques. Commission des Neiges et Glaces.*] *Symposium. Mécanique de la neige. Actes du colloque de Grindelwald, avril 1974*, p. 51–61. (IAHS–AISH Publication No. 114.)

Dufour, L., *and* Defay, R. 1963. *Thermodynamics of clouds. Translated by M. Smyth and A. Beer.* New York and London, Academic Press. (International Geophysics Series, Vol. 6.)

Fletcher, N. H. 1970. *The chemical physics of ice.* Cambridge, University Press. (Cambridge Monographs on Physics.)

Greenwood, G. W. 1956. The growth of dispersed precipitates in solutions. *Acta Metallurgica*, Vol. 4, No. 3, p. 243–48.

Hobbs, P. V. 1968. The metamorphism of dry snow at a uniform temperature. *Union de Géodésie et Géophysique Internationale. Association Internationale d'Hydrologie Scientifique. Assemblée générale de Berne, 25 sept.–7 oct. 1967.* [*Commission de Neiges et Glaces.*] *Rapports et discussions*, p. 392–402. (Publication No. 79 de l'Association Internationale d'Hydrologie Scientifique.)

Hobbs. P. V., *and* Mason, B. J. 1964. The sintering and adhesion of ice. *Philosophical Magazine*, Eighth Ser., Vol. 9, No. 98, p. 181–97.

International critical tables. 1926–33. New York and London, McGraw-Hill Book Co. Inc. 8 vols.

Lifshits, I. M., *and* Slyozov, V. V. 1961. The kinetics of precipitation from supersaturated solid solutions. *Physics and Chemistry of Solids*, Vol. 19, Nos. 1–2, p. 35–50.

Mellor, M. 1968. Avalanches. U.S. Cold Regions Research and Engineering Laboratory. *Cold regions science and engineering.* Hanover, N.H., Pt. III, Sect. A3d.

Paren, J. G., *and* Walker, J. C. F. 1971. Influence of limited solubility on the electrical and mechanical properties of ice. *Nature, Physical Science*, Vol. 230, No. 12, p. 77–79.

Wakahama, G. 1965. Mizu o fukunda sekisetsu no henkei [Metamorphisms of wet snow]. *Teion-kagaku: Low Temperature Science*, Ser. A, [No.] 23, p. 51–66.

Wakahama, G. 1968. The metamorphism of wet snow. *Union de Géodésie et Géophysique Internationale. Association Internationale d'Hydrologie Scientifique. Assemblée générale de Berne, 25 sept.–7 oct. 1967.* [*Commission de Neiges et Glaces.*] *Rapports et discussions*, p. 370–79. (Publication No. 79 de l'Association Internationale d'Hydrologie Scientifique.)

Wakahama, G. [1975.] The role of meltwater in densification processes of snow and firn. [*Union Géodésique et Géophysique Internationale. Association Internationale des Sciences Hydrologiques. Commission des Neiges et Glaces.*] *Symposium. Mécanique de la neige. Actes du colloque de Grindelwald, avril 1974*, p. 66–72. (IAHS–AISH Publication No. 114.)